Systems/Circuits

Differential Muscarinic Modulation in the Olfactory Bulb

Richard S. Smith, Ruilong Hu, Andre DeSouza, Christian L. Eberly, Krista Krahe, Wilson Chan, and Ricardo C. Araneda

Department of Biology, University of Maryland, College Park, Maryland 20742

Neuromodulation of olfactory circuits by acetylcholine (ACh) plays an important role in odor discrimination and learning. Early processing of chemosensory signals occurs in two functionally and anatomically distinct regions, the main and accessory olfactory bulbs (MOB and AOB), which receive extensive cholinergic input from the basal forebrain. Here, we explore the regulation of AOB and MOB circuits by ACh, and how cholinergic modulation influences olfactory-mediated behaviors in mice. Surprisingly, despite the presence of a conserved circuit, activation of muscarinic ACh receptors revealed marked differences in cholinergic modulation of output neurons: excitation in the AOB and inhibition in the MOB. Granule cells (GCs), the most abundant intrinsic neuron in the OB, also exhibited a complex muscarinic response. While GCs in the AOB were excited, MOB GCs exhibited a dual muscarinic action in the form of a hyperpolarization and an increase in excitability uncovered by cell depolarization. Furthermore, ACh influenced the input–output relationship of mitral cells in the AOB and MOB differently showing a net effect on gain in mitral cells of the MOB, but not in the AOB. Interestingly, despite the striking differences in neuromodulatory actions on output neurons, chemogenetic inhibition of cholinergic neurons produced similar perturbations in olfactory behaviors mediated by these two regions. Decreasing ACh in the OB disrupted the natural discrimination of molecularly related odors and the natural investigation of odors associated with social behaviors. Thus, the distinct neuromodulation by ACh in these circuits could underlie different solutions to the processing of general odors and semiochemicals, and the diverse olfactory behaviors they trigger.

Key words: accessory olfactory bulb; aggression; cholinergic; muscarinic; olfactory; social behavior

Significance Statement

State-dependent cholinergic modulation of brain circuits is critical for several high-level cognitive functions, including attention and memory. Here, we provide new evidence that cholinergic modulation differentially regulates two parallel circuits that process chemosensory information, the accessory and main olfactory bulb (AOB and MOB, respectively). These circuits consist of remarkably similar synaptic arrangement and neuronal types, yet cholinergic regulation produced strikingly opposing effects in output and intrinsic neurons. Despite these differences, the chemogenetic reduction of cholinergic activity in freely behaving animals disrupted odor discrimination of simple odors, and the investigation of social odors associated with behaviors signaled by the Vomeronasal system.

Introduction

Throughout the brain, ACh produces a state-dependent regulation of sensory circuits, shaping cognition and behavior (Fournier et al., 2004; Marder, 2012). Cholinergic neurons in the horizontal limb of the diagonal band of Broca (HDB) provide rich innervations to the olfactory bulb (OB) and upstream olfactory areas, where ACh regulates odor processing (Doty et al., 1999; Linster and Cleland, 2002; Wilson et al., 2004; Hellier et al., 2012; Zaborszky et al., 2012; Chapuis and Wilson, 2013; Linster and Fontanini, 2014). Odor cues orchestrate a host of behaviors, including foraging, prey detection, aggression, and sexual bonding. Upon detection by sensory neurons, odors signal through two parallel pathways that synapse onto principal neurons, the mitral and tufted cells (MCs herein) in the main and accessory OB (MOB and AOB, respectively). Unlike other sensory modalities, MCs project directly to higher odor processing areas, bypassing the thalamus, which highlights the importance of top-down cholinergic regulation of OB circuits (Kay and Sherman, 2007; Gire et al., 2013).

Although the role of ACh in enhancing odor discrimination by the MOB is well established (D'Souza and Vijayaraghavan,

Received Jan. 8, 2015; revised May 20, 2015; accepted June 18, 2015.

Author contributions: R.S.S., R.H., A.D., C.L.E., W.C., and R.C.A. designed research; R.S.S., R.H., A.D., C.L.E., W.C., and K.K. performed research; R.S.S., R.H., A.D., and R.C.A. analyzed data; R.S.S. and R.C.A. wrote the paper.

This work was supported by National Institutes of Health/National Institute on Deafness and Other Communication Disorders Grant DCR01-DC-009817 to R.C.A. A.D. was supported by an undergraduate Howard Hughes Medical Institute research fellowship. R.S.S. was supported by a National Science Foundation graduate research fellowship. We thank the members of the R.C.A. laboratory and Nathan Zimnik for their helpful comments.

The authors declare no competing financial interests.

Correspondence should be addressed to Dr. Ricardo C. Araneda, Department of Biology, Bioscience Research Building R-1239, University of Maryland, College Park, MD 20742. E-mail: raraneda@umd.edu.

DOI:10.1523/JNEUROSCI.0099-15.2015

 0270-6474/15/3510773-13$15.00/0

2014), the contribution of neuromodulation of AOB neurons by ACh to behaviors mediated by the vomeronasal system (VNS) is poorly understood. Furthermore, at the cellular and circuit levels, the mechanism of cholinergic modulation, at least in the MOB, remains controversial, and activation of both muscarinic and nicotinic ACh receptors (mAChR and nAChR, respectively) has been shown to either enhance or decrease inhibition in the MOB (Castillo et al., 1999; Ghatpande et al., 2006; Pressler et al., 2007; Zhan et al., 2013). ACh also enhances the excitability of output and intrinsic neurons in the AOB (Smith and Araneda, 2010; Shpak et al., 2014), supporting a functional role for cholinergic inputs in the AOB. At the circuit level, the AOB and MOB appear remarkably similar, both characterized by the presence of ubiquitous reciprocal synapses between MCs and a extensive network of local inhibitory neurons, the granule cells (GCs) (Shepherd and Greer, 1998; Larriva-Sahd, 2008), suggesting that neuromodulators regulate these circuits by similar mechanisms. However, anatomical and functional evidence shows important differences in the connectivity at the level of the sensory input, suggesting that the AOB and MOB analyze chemosensory information differently (Mucignat-Caretta et al., 2012); therefore, neuromodulation by ACh could serve different functions in these related systems.

Here, we show that cholinergic modulation produces distinct and opposite effects on the excitability of neurons in the AOB and MOB. In the AOB, activation of M1-mAChRs directly excites MCs, whereas in the MOB, M2 activation inhibits MCs. Similarly, whereas in the AOB M1 activation depolarized GCs, the response of GCs to ACh in the MOB involved both M1 and M2 mAChRs. Moreover, chemogenetic activation of HDB cholinergic neurons improved the natural discrimination of volatile odors, whereas silencing them disrupted odor discrimination. Importantly, silencing cholinergic neurons also disrupted the investigation of social odors processed by the AOB. Thus, despite the differences in modulation at a network level, decreased ACh affected odor-mediated behaviors signaled through both MOB and AOB, suggesting that neuromodulatory control is dependent on the nature of the chemical signals processed by these regions.

Materials and Methods

Animals. All animal procedures were performed in accordance to the guidelines of the Institutional Animal Care and Use Committee of the University of Maryland. Electrophysiological and behavioral experiments were performed on wild-type strains (C57BL/6, The Jackson Laboratory; Cf1/129S, Charles River) or transgenic mice expressing proteins under the choline acetyltransferase (ChAT) promoter: the ChAT-Cre, ChAT-Tau-GFP, and ChAT-Channelrhodopsin2-YFP lines (ChAT-ChR). The presence of the yellow fluorescent protein (YFP) in the latter allows for direct fluorescence detection of ChR expressing neurons. The ChAT-Cre and ChAT-ChR were obtained from The Jackson Laboratory (stock #006410 and #014546) (Rossi et al., 2011; Zhao et al., 2011). The Chat-Tau-GFP line was generously provided by Dr. Sukumar Vijayaraghavan (Salcedo et al., 2011), and the *M1* and *M1/M3*$^{-/-}$ double knock-out mice were provided by Dr. Jurgen Wess, National Institutes of Health (Gautam et al., 2004). The OMP-YPF mice were obtained from The Jackson Laboratory (stock # 014173) (Shusterman et al., 2011). Experiments were conducted in mice ranging in age from postnatal day 20 (PD20) through 6 months old. Animals were kept on a 12 h light/dark cycle with access to food and water *ad libitum*. Behavioral testing occurred within a 5 h window after the start of the dark phase of the light cycle.

Slice preparation. Electrophysiological recordings were performed in OB slices using methods previously described (Smith et al., 2009). Briefly, after death, the brain was quickly removed and placed in oxygenated ice-cold ACSF containing low Ca^{2+} (1 mM) and high Mg^{2+} (6 mM). Sagittal and horizontal sections (250 μm) of the OB were obtained using a Leica microslicer. Slices were then transferred to an incubation chamber containing normal ACSF (see below) and left to recuperate at 35°C for 30 min, and at room temperature thereafter. For all experiments, the extracellular solution was ACSF of the following composition (in mM): 125 NaCl, 25 $NaHCO_3$, 1.25 NaH_2PO_4, 3 KCl, 2 $CaCl_2$, 1 $MgCl_2$, 3 myo-inositol, 0.3 ascorbic acid, 2 Na-pyruvate, and 15 glucose, continuously oxygenated (95% O_2/5% CO_2). Experiments were performed at room temperature (~25°C).

Data acquisition and analysis. After incubation, the slices were transferred to a recording chamber mounted on the stage of an Olympus BX51 microscope. Recordings were performed using a dual EPC10 amplifier (HEKA) in the current-clamp mode. Fluorescence-labeled neurons were visualized using 10× and 40× LUMPlanFI/IR Olympus water-immersion objectives. Fluorescent illumination was achieved using an OPTOLED (Cairn Research) with blue and white LEDs (blue exciter λ 488 nm, green exciter λ 594 nm, Chroma Technology). Emitted light was collected using an ORCA-Flash4.0 V2 sCMOS camera (Hamamatsu). LED stimulations were commanded using the PatchMaster software (HEKA), and imaging analysis was performed offline using the ImageJ, IgorPro software (Wavemetrics) and MATLAB (MathWorks). Current simulations mimicking *in vivo* synaptic activity were generated with MATLAB software and modeled using neuronal parameters previously described (Galán et al., 2008; Padmanabhan and Urban, 2010). These simulated currents were superimposed onto direct current stimuli of different intensity (−20 to 80 pA) that were randomly interleaved. For ChR light stimulations, the blue light (λ 488 nm) intensity after the 40× objective was placed over the OB was 5 mW/mm^2. Recordings were performed using standard patch pipettes (3–8 MΩ resistance), with an internal solution of the following composition (in mM): 120 K-gluconate, 10 Na-gluconate, 4 NaCl, 10 HEPES-K, 10 Na phosphocreatine, 2 Na-ATP, 4 Mg-ATP, and 0.3 GTP, adjusted to pH 7.3 with KOH. The fluorescent marker AlexaFluor-594 (10 μM, Invitrogen) was included in the pipette solution for reconstruction and *post hoc* analysis of cell morphology using confocal imaging. MCs lacking primary and/or lateral dendrites were not included in the analysis. For Ca-imaging experiments, slices from ChAT-Cre mice expressing hM_4D_i (see below), containing the HDB, were transferred to a Millicell culture dish (Millipore) containing 5 ml of oxygenated ACSF with 5 μM of the calcium indicator Fluo-4 AM (Invitrogen). Slices were submerged in the dye for 20 min and then transferred to the recording chamber. Illumination was achieved using an OPTOLED blue LED (exciter 488 nm center wavelength, Chroma Technology; Cairn Research). The emitted light was collected using an ORCA-Flash4.0 camera (Hamamatsu), and images were recorded using the HCimage software (Hamamatsu). The data in Figure 5*B* correspond to optical recordings of selected HDB neurons responding to clozapine N-oxide (CNO). The ratio of the change in fluorescence with respect to baseline was expressed as $\Delta F/F_0$. Electrophysiology and imaging analysis were performed offline using the ImageJ and IgorPro (Wavemetrics) software. Data values are presented as the mean ± SEM, and statistical significance (p values) for pairwise comparisons were calculated using the Student's t test.

Confocal imaging and immunohistochemistry. Mice were perfused intracardially with 4% PFA; after dissection, the brains were postfixed overnight at 4°C. Subsequently, the brains were placed in PBS and sagittally sliced at 100 μm. Similarly, for MCs fluorescently labeled during electrophysiological recordings, at the end of the experiments, slices were placed in 4% PFA for 20 min at room temperature and then washed overnight in PBS. Cells, and layers of the OB, were visualized using TO-PRO-3 (T3605, Invitrogen) or DAPI (F6057, Sigma-Aldrich). For double-labeling immunofluorescence, free-floating sections (100 μm) obtained in a Vibroslicer (Vibratome Series 1000) were washed twice in PBS and then incubated with 10% donkey serum (Sigma-Aldrich) in 0.1% PBS-Triton X-100 (PBS-T) for 1 h at room temperature. Slices were incubated overnight with one or more of the following primary antibodies, diluted in PBS-T with 2.5% of donkey serum; goat anti-ChAT (1:500, ab144p, Millipore), rabbit anti-vesicular acetylcholine transporter (VAChT, 1:150, ab68984, Abcam), mouse anti-acetylcholinesterase (AChE, 1:100,

ab2803, Abcam), rabbit anti GFP (1:1000, A11122, Invitrogen), and mouse anti-RFP (1:750, ab65856, Abcam). After incubation with the primary antibodies, the samples were washed with PBS-T seven times (5 min each) and then incubated for 2 h at room temperature with the secondary antibody: donkey anti-rabbit Alexa-488 (A-21206, Invitrogen), donkey anti-mouse Alexa-594 (A-21207, Invitrogen), and donkey anti-goat Alexa-488 (A-11055, Invitrogen), all diluted at 1:750 in PBS-T with donkey serum (2.5%). The sections were then washed three times in PBS-T and then four times in regular PBS (5 min each). To visualize immunofluorescence, slices were mounted with Vectashield (Vector Laboratories) and imaged with a Leica SP5× confocal microscope (Leica Microsystems). Confocal imaging reconstructions and analysis were performed using the Leica software and ImageJ. For analysis of the density of ChAT-positive (ChAT$^+$) fibers in the OB (see Fig. 4), we used an anti-GFP antibody to enhance the signal. The same antibody was used in OB slices of OMP-YFP mice. Reconstructions were produced from stacked confocal images (63×, 50 μm in the *z* plane) and fluorescence intensity profiles were generated along a randomly selected 10-μm-wide ROI. Fluorescence intensity values were quantified for the glomerular layer (GL), mitral cell layer (MCL), and granule cell layer (GCL). Analysis of axonal fiber density in the OB was performed as previously described (Krosnowski et al., 2012). Briefly, the raw images are filtered (5px median filter) and normalized to the peak values for each image. We then determined the average fluorescence intensity (normalized pixel intensity) across each layer.

Stereotaxic viral injections. Expression of the hM_4D_i and hM_3D_q DREADDS in ChAT-Cre mice was achieved by stereotaxic targeted injections (1 μl) of the adenovirus AAV8-hSyn-DIO-hM3D (Gq)-mCherry or AAV8-hSyn-DIO-hM4D (Gi)-mCherry (University of North Carolina vector core) bilaterally into the HDB. Anesthetized mice (1.5% isoflurane) were head-fixed (model 900, Kopf Instruments) and a 33-gauge needle (5 μl syringe, Hamilton) was inserted through a 1 mm craniotomy window. The speed of virus injection (100 nl/min) was achieved by using a syringe pump (Micro4 Microsyringe pump, World Precision Instruments). Injection in the HDB was targeted using the following coordinates, in relation to bregma (in mm): dorsoventral axis −5.4, mediolateral ±1.625, anteroposterior 0.14. Virus injections occurred at PD30 and behavioral experiments were conducted beginning 6 weeks after the virus injection. We note that, at 6 weeks after injection, the presence of the DREADDs can be readily detected using antibodies (see Fig. 5*A*); however, the red fluorescence (mCherry) in live tissue is very low, making the targeted patch recordings difficult.

Behavioral tests for natural odor discrimination. Odor discrimination was tested using the habituation/dishabituation paradigm as previously described (Nunez-Parra et al., 2013). Briefly, ChAT-Cre mice virally transfected with hM_4D_i or hM_3D_q received an intraperitoneal injection of PBS (control) or the biologically inert ligand CNO (0.5 mg/1 ml/100 g, treated). Activation of DREADDS with CNO allows for modulation of HDB cholinergic neurons at physiological levels, with optimal behavioral effects observed 2 h after CNO injection (Sternson and Roth, 2014). Ninety minutes after injection, mice were placed in a clean cage (20 cm × 40 cm) in the presence of an unscented wooden block for 30 min. Following this familiarization period, both groups were tested for their ability to discriminate between the following odor pairs: ethyl heptanoate (C7)/ethyl octanoate (C8), ethyl hexanoate (C6)/ethyl octanoate (C8), L-carvone/D-carvone and α-pinene/β-pinene. During the habituation phase, each mouse was exposed during three consecutive trials to a wooden block scented with 100 μl of the first odor (1:1000 dilution). The fourth exposure consisted of the test odor (dishabituation); each exposure lasted 2 min, with a 1 min intertrial interval. Each trial was videotaped for off-line quantification of the time the mouse spent investigating the block. The investigation time was defined as the total time when the mouse's nose was within a 2 cm radius of the wooden block. For assessment of odor threshold in the ChAT-hM_4D_i and hM_3D_q mice, C7 was tested at increasing odor concentrations (1:60,000; 1:40,000; 1:30,000; 1:20,000) following three presentations of a block "scented" with distilled water. Odor discrimination was considered successful when mice showed a significant increase in investigation during the presentation of the test odor (C7).

Behavioral tests for natural investigation of male and female odors. Assessment of aggression-induced avoidance of conspecific odors in males was conducted using a modified resident-intruder paradigm (Koolhaas et al., 2013). Sexually naive ChAT-hM_4D_i mice (intruders) and background-matched CF1/129S mice (residents) were housed in isolation for 2 weeks before the experiments. Following the isolation period, experiments were performed in a neutral environment (20 cm × 40 cm cage), and soiled bedding from a conspecific was presented in a Petri dish (100 × 15 mm) for 15 min. Ninety minutes after injection of PBS, or CNO, the ChAT-hM_4D_i intruder mice were presented again with soiled bedding from a resident male. Next, ChAT-hM_4D_i intruder mice undergo an aggressive encounter with the resident in which the ChAT-hM_4D_i intruder is defeated. Following the aggressive encounter, the ChAT-hM_4D_i intruder is returned to the neutral test arena and presented again with the soiled bedding from the resident mouse. To assess male preference for female bedding, male ChAT-hM_4D_i mice were first placed in the test arena in the presence of male-soiled bedding as a control. Next, they were presented with female-soiled bedding (15 min each). In our assays, male mice always show preference for female bedding, regardless of whether they are presented with male bedding first or second. Female-soiled bedding was obtained from group-housed, sexually naive, age-/background-matched mice (CF1/129S). All social experiments were conducted in complete darkness and filmed using a camera with IR sensitivity for offline analysis (Full Spectrum 1080p IR Camera, Cleveland Paranormal Supply). Mice trajectories were analyzed using a custom MATLAB tracking software. Data shown in Figure 6 are presented as a ratio from Trial 2 to Trial 1 (Trial 2/Trial 1) of the average distance from the dish the intruder spent during the trial. Larger absolute values for the ratio indicate preference or avoidance for the soiled bedding. Quantifications of stereotypic social behaviors were performed by a blind observer and quantified as the total duration (seconds) within the 15 min investigation trial. The behaviors quantified included the following: investigating (mouse nose in downward position on/in the Petri dish), exploring (traversing cage, digging, climbing on walls, nondescript movement), grooming, and freezing.

Behavioral test for novel object recognition. The two sample, one environment, version of the novel object recognition task was used following the protocol (Bevins and Besheer, 2006). The training objects used were two blue marbles, and the novel object used was a yellow wooden cube of approximately similar size. Before the novel object recognition task, ChAT-hM_4D_i mice were familiarized to the testing arena for 10 min during 2 consecutive days. For novel object recognition, the training period was 10 min, followed by a 45 min interval before a 5 min testing period. CNO injections were administered 2 h before the start of training. The familiarization, training, and testing periods were filmed and analyzed in custom MATLAB software to quantify investigation times and motor behavior in general.

Solutions and pharmacological agents. The following drugs were bath applied: CNQX, APV, 11-[[2-[(diethylamino)methyl]-1-piperidinyl] acetyl]-5,11-dihydro-6*H*-pyrido[2,3-*b*][1,4]benzodiazepin-6-one (AFDX-116), [*S*-(*R**,*R**)]-[3-[[1-(3,4-dichlorophenyl)ethyl]amino]-2-hydroxypropyl](cyclohexylmethyl) phosphinic acid (CGP-54626), (−)-nicotine ditartrate (Nic), and *N*,2,3,3-tetramethylbicyclo[2.2.1]heptan-2-amine hydrochloride (MM), TTX. For electrophysiology recordings, the speed of perfusion permitted for full solution exchange of the recording chamber in <30 s. However, the reported values of "time to peak" are an overestimate, as we do not subtract the dead volume in the perfusion line, which also adds to the total time it takes the agonist to reach the recorded neuron. Therefore, in a few experiments, we conducted experiments using local perfusion of drugs (AutoMate Scientific). Antagonists were applied for at least 10 min before the application of the agonist. All drugs were purchased from Tocris Bioscience unless otherwise indicated. CNO (Enzo Life Science) was prepared fresh daily in PBS at 0.5 mg/ml and injected at 0.5 mg/100 g. All odors used for behavior experiments were purchased from Sigma-Aldrich.

Results

Muscarinic cholinergic activation produces opposite effects of output neurons of the AOB and MOB

To determine the neuromodulatory effects of ACh on OB output neurons, we examined the actions of selective mAChRs on MCs of the AOB and MOB (Fig. 1). In agreement with our previous work (Smith and Araneda, 2010), application of the nonselective mAChR agonist oxotremorine (oxo, 10 μM) produced a robust depolarization in AOB MCs, which usually elicited firing (Fig. 1*B*; ΔV_m, 15.4 ± 2.7 mV, $n = 28$, $p < 0.01$). Surprisingly, in the MOB, the same agonist treatment produced a significant inhibition of MCs (top, ΔV_m, −2.2 ± 0.5 mV, $n = 17$, $p < 0.01$). The time course of these muscarinic responses in the MOB and AOB MCs exhibited slow kinetics (time to peak, MOB, 41.6 ± 6.8 s, $n = 17$, AOB, 71.4 ± 8.8 s, $n = 28$, $p < 0.01$). However, these values are an overestimate (see Materials and Methods); thus, in a few experiments, we applied oxo (30 μM) in the vicinity of the recorded cell, using a fast perfusion system. Under these conditions, the time to peak was 31.1 ± 5.7 s in the MOB and 21.3 ± 4.5 s in the AOB ($n = 5$).

To rule out the possibility that the inhibitory response in the MOB was disynaptic in origin, we examined the effects of oxo in the presence of blockers of fast excitatory and inhibitory synaptic transmission (APV 100 μM, CNQX 10 μM, and GABAzine, 5 μM). As previously shown for the excitatory response in the AOB (Smith and Araneda, 2010), the muscarinic inhibition in the MOB was not affected by the presence of the ionotropic receptor blockers, indicating a direct effect on MCs (ΔV_m, oxo, −2.4 ± 0.6 mV, oxo + blockers, −2.1 ± 0.4 mV, $n = 8$, $p = 0.68$). Furthermore, in the presence of the ionotropic blockers, the time to peak of the responses remained unchanged (MOB, oxo 40.8 ± 8.3 s, oxo + blockers 45.1 ± 6.6 s, $n = 8$, $p = 0.7$). Similarly, the $GABA_B$ receptor antagonist (CGP-54626, 5 μM) did not block the hyperpolarization in MCs of the MOB (ΔV_m, oxo −2.7 ± 0.5 mV, oxo + CGP −2.4 ± 0.2 mV, $n = 5$, $p = 0.52$). In addition, as previously reported, nicotine (Nic, 10 μM) produced a fast depolarization in both MOB and AOB MCs (time to peak, MOB, 24.4 ± 4.7 s; AOB, 30.1 ± 6.3 s) (Smith and Araneda, 2010; D'Souza and Vijayaraghavan, 2012). Like the muscarinic effect, the nicotinic depolarization was not affected by blockers of fast synaptic transmission (ΔV_m, AOB, Nic 11.1 ± 0.9, Nic + blockers 12.6 ± 1.3, $n = 12$, $p = 0.77$; ΔV_m, MOB, Nic, 9.3 ± 2.0, Nic + blockers, 11.3 ± 2.5, $n = 11$, $p = 0.68$), indicating the direct activation of nAChRs on MCs. Last, the oxo (10 μM)-induced depolarization in the AOB and the hyperpolarization in the MOB were not affected by the nonselective nicotinic antagonist, mecamylamine (MM, 30 μM) (ΔV_m oxo + MM, AOB, 15.9 ± 3.2 mV, $n = 3$; MOB, −3.2 ± 0.4 mV, $n = 3$).

We have previously shown that the muscarinic depolarization in AOB MCs results from M1-mAChR activation (Smith and Araneda, 2010). However, a low concentration of pirenzepine (Pir, 300 nM), which selectively blocks M1-mAChRs, was ineffective in reducing the inhibitory response in MOB MCs (Fig. 1*C*; ΔV_m, oxo + Pir, −2.9 ± 0.8 mV, $n = 5$). To further corroborate these findings, we examined MC responses in the M1 knock-out mice ($M1^{-/-}$ KO mice). Unexpectedly, the inhibitory responses in MOB MCs, but also the excitatory response in AOB MCs, still persisted in the $M1^{-/-}$ KO mice. Pharmacological characteriza-

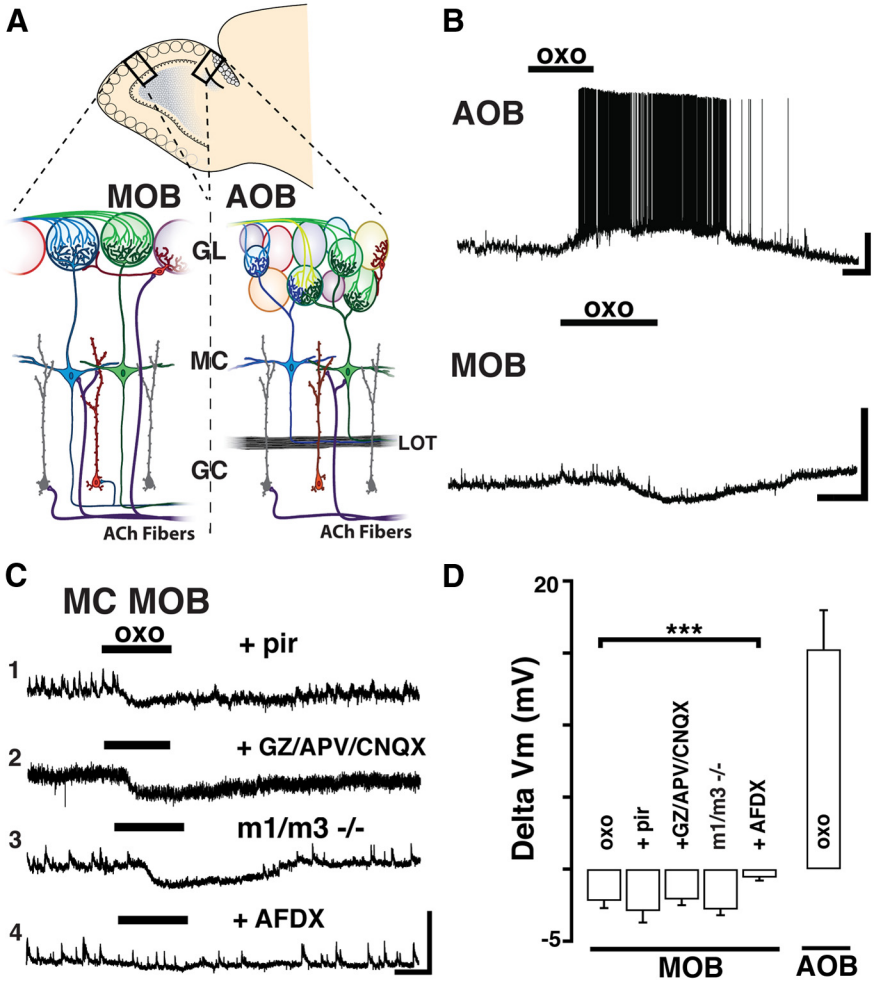

Figure 1. Muscarinic receptor activation produces opposite effects on mitral cells of the AOB and MOB. ***A***, Diagram of a sagittal view of the OB. Magnified sections enclosed by the black rectangles are shown below. Left, MOB. Right, AOB. In the glomerular layer (GL), sensory axons (green and blue) relay information to output neurons residing in the MCs (blue and green). GCs (red and gray) are the most abundant cells in the MOB and AOB and form dendrodendritic synapses with MCs, influencing bulbar output through GABAergic inhibition. Cholinergic fibers arising from the basal forebrain (ACh fibers, purple) innervate both the MOB and AOB. LOT, Lateral olfactory tract. ***B***, Current-clamp recordings from MCs shows opposite effects of the muscarinic ACh receptor (mAChR) agonist oxotremorine (oxo,10 μM, here and in all figures); a depolarization in the AOB (top) and hyperpolarization in the MOB (bottom); the resting membrane potential in these MCs is −57 and −59 mV, respectively. Calibration: top, 20 mV, 1 min; bottom, 10 mV, 1 min. ***C***, Examples of responses to oxo in MOB MCs under different conditions. ***C1***, The hyperpolarizing response to oxo is unchanged in the presence of M1-mAChR antagonist pirenzepine (Pir, 300 nM, $V_m = -59$ mV) or in the presence of ionotropic glutamate receptor (iGluR) blockers and GABA antagonist (***C2***, APV 100 μM, CNQX 10 μM, and GABAzine 5 μM, $V_m = -55$ mV). ***C3***, The hyperpolarization persisted in MOB MCs from *M1/M3* $^{-/-}$ KO mice ($V_m = -58$ mV). However, the oxo-induced hyperpolarization is abolished in the presence of an M2-mAChR antagonist AFDX-116 (***C4***, 300 nM, $V_m = -57$). Calibration: all traces, 10 mV, 1 min. ***D***, Summary of the effects produced by oxo on MC excitability in the MOB and AOB. The muscarinic hyperpolarization in MOB MCs is sensitive to AFDX-116. ***$p < 0.01$.

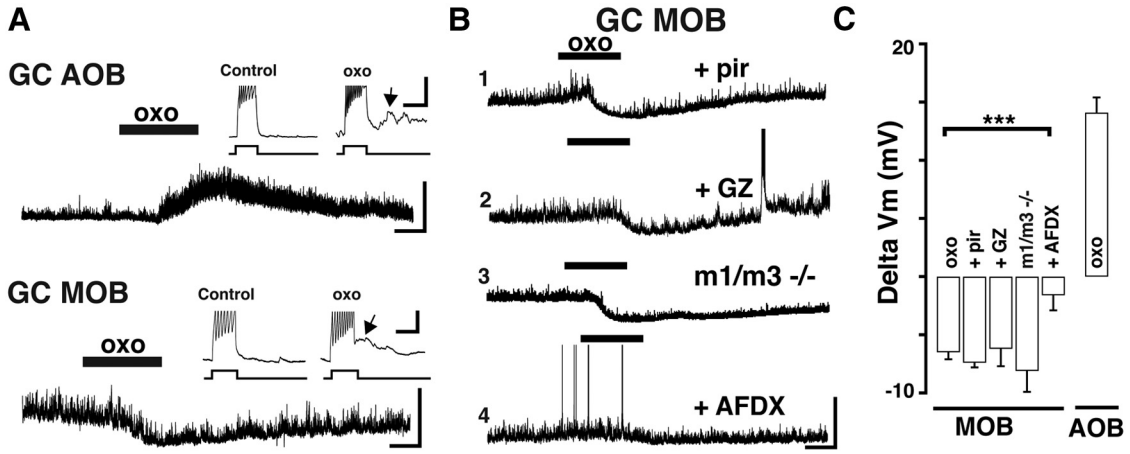

Figure 2. Activation of M2 muscarinic receptors hyperpolarizes MOB GCs. ***A***, Current-clamp recordings from GCs showing opposite muscarinic effects in the AOB and MOB. In the AOB (top) oxo produces a depolarization, whereas in the MOB (bottom) oxo produces a hyperpolarization. $V_m = -62$ mV (top) and $V_m = -61$ mV (bottom). Calibration: 20 mV, 1 min. Inset, The 25 pA current injections reveal an increase in excitability and the appearance of a sADP (arrows). Calibration: 5 mV, 0.5 s. ***B***, Examples of responses to oxo in MOB GCs under different conditions. ***B1***, The hyperpolarization was not affected by Pir (300 nM, $V_m = -61$ mV) or by the GABA antagonist GABAzine (***B2***, GABAzine, 5 μM, $V_m = -62$ mV). ***B3***, oxo still produced a robust hyperpolarization in *M1/M3* $^{-/-}$ KO mice ($V_m = -60$ mV). However, the hyperpolarization was abolished in the presence of the M2-mAChR antagonist AFDX-116 (***B4***, 300 nM, $V_m = -61$ mV). Calibration: all traces, 20 mV, 1 min. ***C***, Summary of the properties of muscarinic response of GCs in the MOB and AOB. The muscarinic hyperpolarization in MOB GCs is sensitive to AFDX-116. ***$p < 0.01$.

tion indicated that the depolarization in AOB MCs was sensitive to M3-mAChRs blockers, suggesting an upregulation of these receptors in the OB of *M1* $^{-/-}$ KO mice (data not shown). Therefore, we next conducted experiments in the M1/M3 double KO mice (*M1/M3* $^{-/-}$). As shown in Figure 1*C*, oxo still elicited a hyperpolarization in MOB MCs (ΔV_m, -2.8 ± 0.6 mV, $n = 5$, $p = 0.82$), whereas the oxo-induced excitation in AOB MCs was completely absent in the *M1/M3* $^{-/-}$ mice (ΔV_m, -0.2 ± 0.1 mV, $n = 4$, $p < 0.01$; data not shown). Additional pharmacological experiments revealed that the hyperpolarization in MOB MCs results from activation of M2-mAChRs. Accordingly, the inhibitory response to oxo was significantly reduced (8 of 9 cells) in the presence of a submicromolar concentration (300 nM) of AFDX-116 (Fig. 1*C*; ΔV_m, control, -3.1 ± 0.4 mV, oxo + AFDX-116, -0.6 ± 0.2 mV, $n = 8$, $p < 0.01$). In summary, M1-mAChR activation in AOB MCs produces a depolarization. In contrast, M2-mAChR activation in MOB MCs produces an opposite effect (i.e., hyperpolarization). In both MOB and AOB, MCs also exhibit a nAChR-mediated excitation; however, we focus the scope of this work on muscarinic mediated effects.

We wondered whether the opposite effects in muscarinic modulation extended also to the regulation of GCs, the most abundant intrinsic neuron in the OB. In agreement with our previous work (Smith and Araneda, 2010), activation of M1 mAChRs produced an increase in excitability of GCs in the AOB, consisting of a depolarization and the appearance of a slow afterdepolarizing current (sADP) following a stimulus-induced train of action potentials (Fig. 2*A*; ΔV_m, 14.1 ± 1.3 mV; sADP, 5.8 ± 0.4 mV, $n = 9$). In contrast, in MOB GCs, oxo (10 μM) produced a hyperpolarization (Fig. 2*A*; ΔV_m, -6.5 ± 0.6 mV, $n = 8$). This hyperpolarization persisted in the presence of GABAzine (5 μM), ruling out the involvement of a $GABA_A$-mediated inhibition (Fig. 2*B*; ΔV_m, -6.2 ± 1.5 mV, $n = 3$, $p = 0.83$). Additionally, the hyperpolarization in MOB GCs was not reduced by application of a low concentration of Pir (300 nM; Fig. 2*B*; ΔV_m, -7.4 ± 0.4 mV, $n = 4$, $p = 0.41$). However, application of AFDX-116 (300 nM) produced a significant decrease in the hyperpolarization elicited by oxo (Fig. 2*B*; ΔV_m, -1.5 ± 1.3 mV, $n = 5$, $p < 0.01$). Furthermore, like the inhibitory response in MOB MCs, the hyperpolarization in GCs was still present in *M1/M3* $^{-/-}$ mice (Fig. 2*B*; ΔV_m, -8.1 ± 2.0 mV, $n = 5$, $p = 0.36$). A previous report indicated the activation of sADP in MOB GCs, which like the response in AOB GCs, is dependent on activation of M1 mAChRs (Pressler et al., 2007). To examine this possibility, we elicited a train of action potentials with a depolarizing current while using a constant current injection to maintain the membrane potential at ~ -60 mV, thus counteracting the M2-mediated inhibition. In the presence of oxo, a stimulus-induced train of spikes was followed by a sADP in 5 of 7 cells (Fig. 2*A*, inset; ΔV_m, 10.6 ± 1.2 mV, $n = 5$). Importantly, in all GCs, the number of action potentials induced by a stimulus increased during the application of oxo (Fig. 2*A*, inset; action potentials 15.6 ± 1.2 to 26.2 ± 1.8 Hz, $n = 7$, $p < 0.01$). These data suggest that muscarinic activation of MOB GCs produced two opposing effects: an M2-mediated hyperpolarization and an M1-mediated increase in excitability. In contrast, as shown previously, activation of M1-mAChRs alone produces a large increase in GCs excitability in the AOB (Smith and Araneda, 2010).

Optogenetic activation of HDB cholinergic projections reveals opposing actions of acetylcholine on output neurons of the AOB and MOB

HDB cholinergic neurons are regulated in a behavioral state-dependent manner, displaying neuronal bursting during active states and synchronization with γ and θ oscillations (Manns et al., 2000; Lee et al., 2005; Parikh and Sarter, 2008). To examine the mechanisms by which endogenous release of ACh regulates the activity of output neurons, we used a transgenic line that coexpresses ChR and YFP in cholinergic neurons of the HDB. Immunostaining ChR-YFP-positive neurons (ChR-YFP$^+$) with a ChAT primary antibody showed that $\sim$99% of ChR-YFP$^+$ neurons (93 ± 12 cells/mm^2, $n = 6$) colabeled for ChAT (92 ± 9 cells/mm^2, $n = 6$), indicating a robust ChR expression in HDB cholinergic neurons. Moreover, the distribution pattern of ChR-YFP$^+$ fibers in the OB (data not shown) closely resembled the distribution pattern of fibers in another transgenic mouse, the ChAT-Tau-GFP (see Fig. 4*A*). As shown in Figure 3*A*, prolonged blue light stimulation over the OB (λ 488 nm, 5 mW, 10 Hz, 50 ms pulses, 30 s) reliably elicited action potentials in ChAT-YFP-ChR$^+$ neurons in the HDB ($95 \pm 2.1\%$ success; Fig. 3*A*). We next

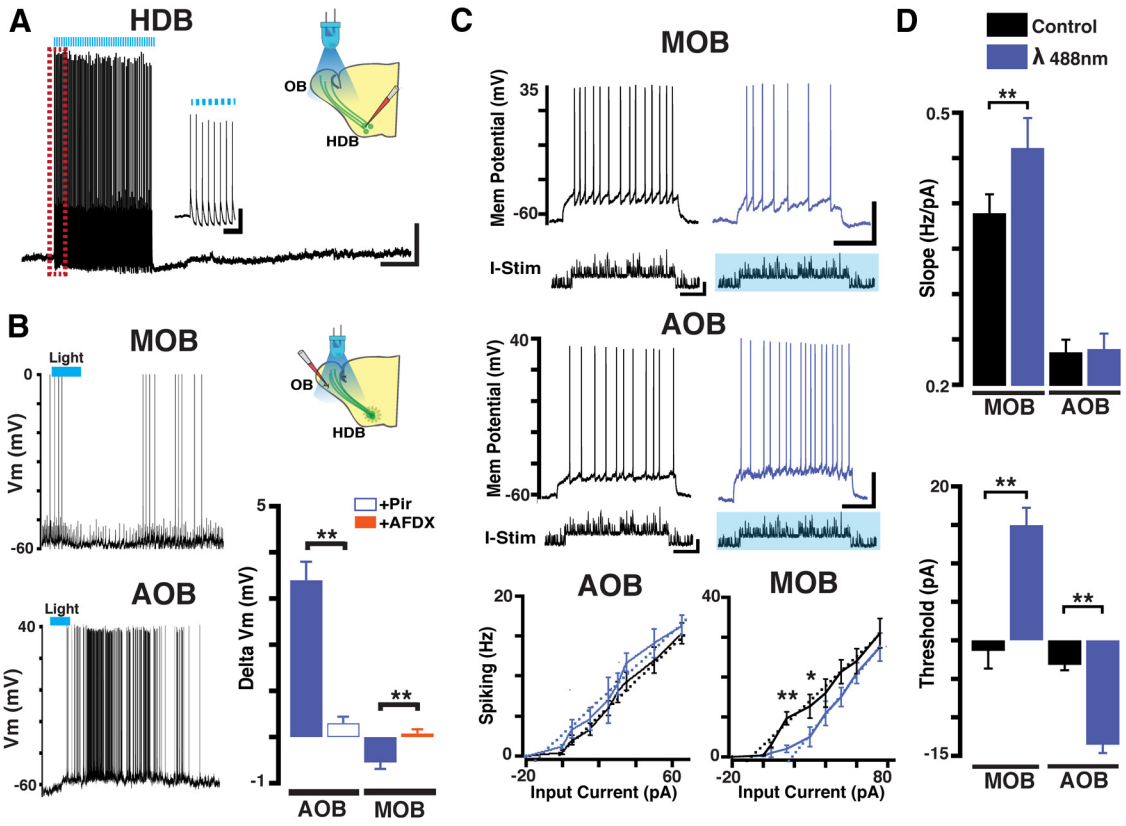

Figure 3. Optogenetic activation of HDB cholinergic projections reveals opposing actions of acetylcholine on output neurons of the AOB and MOB. ***A***, Current-clamp recording in a ChAT-ChR-YFP $^+$ neuron in the HDB; consecutive stimulation pulses with blue light (λ 488 nm, blue bar, 10 Hz, 50 ms, 30 s) reliably excited this neuron. Calibration: 20 mV, 1 min. Left inset, Expanded time scale showing the light-evoked action potentials during the time highlighted by the red rectangle; all light pulses induced an action potential in this cell. Calibration: 20 mV, 400 ms. $V_m = -60$ mV. ***B***, Top, Current-clamp recording from a MC in the MOB; optogenetic stimulation (10 Hz, 50 ms duration, 15 s) of ChAT-ChR fibers revealed a small hyperpolarization ($V_m = -59$ mV). Bottom, Recording from an MC in the AOB; optogenetic stimulation produced a depolarization of this MC ($V_m = -62$ mV). Bar graph represents a summary of the pharmacology of the optogenetically elicited responses in MCs. The depolarization in the AOB is abolished by Pir (300 nM), whereas the hyperpolarization on the MOB is sensitive to AFDX. ***A***, ***B***, Right diagrams represent the recording configuration indicating the position of the light stimulus in relation of to the recorded cell (i.e., HDB vs OB). ***C***, Current-clamp recording of an MC in the MOB (top) and in the AOB (bottom). Neuronal spiking was elicited by injection of modeled excitatory synaptic currents overlying square current pulses (I-Stim; see Materials and Methods), in control (black traces) and in the presence of light stimulation (blue traces). The stimulus duration is 2 s, and the amplitude is 25 pA in the MOB and 15 pA in the AOB ($V_m = -58$ mV and $V_m = -60$ mV in the MOB and AOB, respectively). Bottom, Average firing frequency of MCs in response to increasing current stimuli in the AOB (left) and MOB (right). Dotted lines (black represents control; blue represents light stim) indicate the best fit to the rising phase of the current-voltage curves. ***D***, Top, Quantification of the gain, measured by the slope (Hz/pA) of the curves shown in ***C***. Bottom, quantification of MC spiking threshold obtained from the *x*-intercept (pA) of the regression fit to the slope of the relationships shown in ***C***. $^*p < 0.05$. $^{**}p < 0.02$.

recorded from MCs while eliciting release of endogenous ACh with blue light (10 Hz, 50 ms duration, 15 s); a similar stimulation protocol was previously shown to elicit evoked cholinergic responses in the OB (Ma and Luo, 2012; Rothermel et al., 2014). As shown in Figure 3*B*, endogenous ACh elicited a small, but consistent, hyperpolarization in MOB MCs (ΔV_m, -0.7 ± 0.3 mV, $n = 7$, $p < 0.05$), whereas the same light stimulation protocol produced a depolarization in AOB MCs (ΔV_m, 4.3 ± 0.5 mV, $n = 7$, $p < 0.01$). Importantly, in agreement with the pharmacological studies, Pir (300 nM) completely abolished the light-induced excitation in AOB neurons (ΔV_m AOB, light, 3.4 ± 0.4 mV, light + Pir 0.31 ± 0.54 mV, $n = 6$, $p < 0.01$; Fig. 3*B*). Similarly, AFDX (300 nM) reduced the light-induced hyperpolarization in MOB MCs (ΔV_m MOB, light, -0.5 ± 0.14 mV, light + AFDX 0.08 ± 0.09 mV, $n = 5$, $p < 0.05$). Together, these results indicate that the optogenetic-induced responses in MCs were mediated by muscarinic receptors.

Cholinergic modulation has an important role in gating of visual, auditory, and somatosensory information (Niell and Stryker, 2010; Marguet and Harris, 2011; Petersen, 2014). The opposite changes in output neuron excitability elicited by ACh suggested that cholinergic modulation could have a different role in sensory gating in the MOB and AOB. To examine this possibility, we recorded responses of MCs to modeled excitatory potentials that occur in MCs during odor sniffing (see Materials and Methods) in the presence of endogenous ACh release. Simulated synaptic currents were superimposed on current stimuli of different intensity while concurrently stimulating with light (Fig. 3*C*; I-stim, -20 pA to 80 pA). In the MOB, the effect of light stimulation was dependent on the intensity of current used to depolarize MCs. At low current intensities (pA < 30), light stimulation produced a significant decrease in MC firing ($-71 \pm 26\%$, $n = 6$, $p < 0.01$); but at higher current intensities (pA > 50), there was no effect on MC firing ($-5 \pm 19\%$, $n = 6$, $p = 0.85$). In contrast, the firing frequency of MCs in the AOB was consistently higher across the range of current stimuli tested, albeit due to variability in the analyzed sample, it did not reach significance (pA < 30, $15 \pm 7\%$; $p = 0.07$; pA > 50, $5.5 \pm 12\%$, $p = 0.65$, $n = 5$).

We next determined neuronal gain by measuring the slope of linear regression fit to the rising phase of the input–output curves (Chance et al., 2002). As shown in Figure 3*C*, endogenous ACh produced a significant shift in the slope (Hz/pA) in the MOB (Hz/pA, control, 0.36 ± 0.02, blue light, 0.46 ± 0.03, $n = 6$, $p < 0.02$), but not

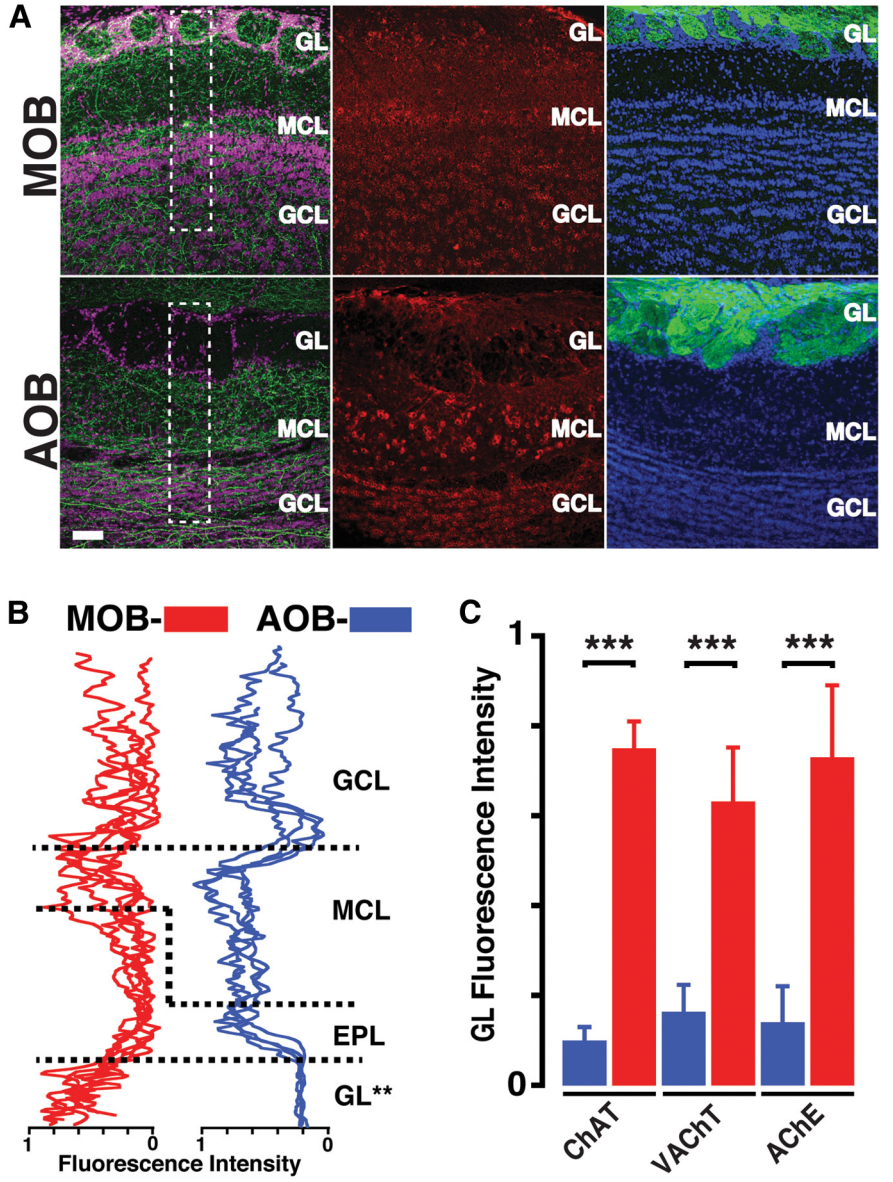

Figure 4. Cholinergic afferent fiber density is differentially distributed in the AOB and MOB. ***A***, High-magnification confocal images of the MOB (top) and AOB (bottom) sections stained for different markers. Left, Sections from a ChAT-Tau-GFP mouse brain, stained with anti-GFP (green) and nuclear stain TOPRO (pink). The ChAT-GFP fibers are found in all layers of the MOB but are absent in the GL of the AOB. Middle, Sections from a wild-type mouse brain stained with anti-VAChT (red). The VAChT staining is prominent in the MOB GL but not in the AOB. Right, Sections from an OMP-YFP mouse, stained with anti-GFP (green) and DAPI (blue). There is abundant labeling in the glomerular layers of the MOB and AOB. Scale bar, 50 μm. ***B***, Fluorescence intensity line plots from the regions outlined in ***A*** (white dotted rectangles; see Materials and Methods) for the MOB (red) and AOB (blue). Each line indicates sections obtained from different animals. In all sections, the intensity is lowest in the GL of the AOB. ***C***, Bar graph represents normalized fluorescence intensity in the GL of MOB (red) and AOB (blue) for different cholinergic markers. All the markers show low intensity in the AOB. $^{**}p < 0.02$. $^{***}p < 0.01$.

in the AOB (Hz/pA, control, 0.24 ± 0.01, blue light, 0.24 ± 0.02, $n = 5$, $p = 0.86$). Furthermore, in the presence of endogenous ACh, the x-intercept (pA) of lines fitted to the input output is shifted toward larger (more positive) input values in the MOB, but require less input (more negative) current the AOB (MOB control, −0.3 ± 2.3 pA, blue light, 14.9 ± 2.3 pA, $n = 6$, $p < 0.01$; AOB control, −3.2 ± 0.7 pA, blue light, −13.5 ± 1.1 pA, $n = 5$, $p < 0.01$). Together, these results indicate that cholinergic neuromodulation produces a nonlinear inhibitory effect on output neurons in the MOB, but a linear increase in excitation in AOB MC, suggesting that neuronal gain is modulated in the MOB but not in the AOB.

Cholinergic afferent fibers are absent in the glomerular layer of the AOB

The above results revealed significant differences in cholinergic modulation in the MOB and AOB, specifically in regards to the contribution of M1 and M2 mAChRs to the regulation of these circuits. Surprisingly, confocal analysis of a transgenic line expressing the Tau-GFP fusion protein under the ChAT promoter (ChAT-Tau-GFP mouse) revealed a divergence in the distribution pattern of cholinergic fibers between the MOB and AOB. In agreement with previous findings (Salcedo et al., 2011; Krosnowski et al., 2012), confocal analysis revealed the presence of ChAT-GFP-positive (ChAT-GFP$^+$) fibers across all layers of the MOB, albeit with different degrees of intensity (Fig. 4*A*). Similarly, in the AOB, the distribution of fibers exhibited various degrees of intensity; however, there was a significant absence of cholinergic fibers in the GL (Fig. 4*A*). To quantify the distribution pattern of cholinergic fibers across the distinct layers of the MOB and AOB, we analyzed fluorescence intensity (ChAT fibers) across the complete dataset (see Materials and Methods). As shown in Figure 4*B*, the intensity was lowest in the GL of the AOB, but there was abundant fluorescence in the GL of the MOB. The average intensity in the GL was significantly different between the AOB and MOB (AOB, 0.08 ± 0.04; $n = 6$; MOB, 0.77 ± 0.09; $n = 6$; $p < 0.01$). This differential pattern of labeling was also observed when we used additional cholinergic markers, the VAChT (AOB vs MOB, 0.17 ± 0.06 vs 0.65 ± 0.11; $n = 4$; $p < 0.01$; Fig. 4*C*) and AChE (AOB vs MOB, 0.15 ± 0.08 vs 0.73 ± 0.16; $n = 4$; $p < 0.01$; Fig. 4*C*). In contrast, as shown in Figure 4*A*, the fluorescence intensity in the AOB GL was high, when we used an anti-GFP antibody in slices from an OMP-YFP mouse, suggesting that the glomerular neuropil in the AOB was accessible to the antibodies. The differential distribution of cholinergic fibers at the level of the GL, where MCs form synapses with incoming sensory fibers, suggests that ACh may play a lesser direct role in regulating synaptic processes in the glomeruli of the AOB.

Modification of HDB cholinergic neuron activity affects natural discrimination of odors

At the network level, our findings suggest a differential effect of ACh in the MOB and AOB; thus, we wondered whether cholinergic modulation has a different role in odor-mediated behaviors signaled by these parallel chemosensory circuits. To modify the cholinergic tone in the OB of awake behaving animals, we used a chemogenetic approach, using Designer Receptors Exclusively Activated by Designer Drugs (DREADDs). This allows for site-

specific expression of genetically modified GPCRs (hM3Dq and hM4Di), which activate distinct cellular mechanisms to excite and inhibit neurons in the presence of CNO, a biologically inert compound that binds DREADD receptors (Armbruster et al., 2007). As shown in Figure 5*A*, 6 weeks after virus injection, hM3Dq and hM4Di DREADDs show robust expression in the HDB (Fig. 5*A*). Double immunostaining against ChAT (green) and the DREADDs (mCherry) indicated that 59 ± 9% of the ChAT-positive (ChAT$^+$) neurons also expressed hM4Di ($n = 4$), whereas 70 ± 11% of ChAT$^+$ neurons expressed hM3Dq ($n = 4$). As shown in Figure 5*B*, 2 weeks after injection, HDB cholinergic neurons expressing hM4Di were inhibited in the presence of CNO (5 μM) (baseline; 1.1 ± 0.3 Hz; CNO, 0.4 ± 0.4 Hz, $n = 3$, $p < 0.02$). Additionally, 4 weeks after injection, we conducted Ca-imaging recordings in HDB neurons expressing hM3Dq. As shown in Figure 5*B*, CNO produce increases in calcium signals in these neurons ($\Delta F/F_0$, 11.6 ± 0.55%, $n = 6$, $p < 0.01$).

To validate our chemogenetic approach, we evaluated the natural discrimination of structurally similar odors using a habituation/dishabituation. This odor discrimination task has traditionally assessed the contribution of ACh to MOB processing (Mandairon et al., 2006; Chaudhury et al., 2009). As shown in Figure 5*C*, ChAT-hM4Di mice injected with saline habituated to three consecutive presentations of ethyl heptanoate (C7) as shown by a decrease in investigation time (first trial 10.01 ± 0.42 s vs third trial, 2.14 ± 0.38 s; $n = 4$, $p < 0.01$). Presentation of the novel odor, ethyl octanoate (C8), resulted in a significant increase in investigation time or dishabituation (Fig. 5*C*; C7 2.14 ± 0.38 vs C8 8.82 ± 0.49 s, $n = 4$, $p < 0.01$). ChAT-hM4Di mice injected with the CNO (0.5 mg/1 ml/100 g) displayed normal habituation to C7 (first trial 9.7 ± 1.0 s vs third trial, 4.0 ± 0.4 s; $n = 4$, $p < 0.01$) but failed to dishabituate to the C8 ester (C7, 4.0 ± 0.4 s vs C8, 3.7 ± 0.6 s, $p = 0.81$), indicating that these mice did not discriminate these odors when the cholinergic activity is reduced. This disruption in odor discrimination was reversible and following the washout of CNO (~5 h), ChAT-hM4Di mice showed normal habituation/dishabituation for the C7/C8 odor pair (C7, 3.8 ± 0.5 s vs C8, 6.2 ± 0.4 s, $p < 0.02$). Furthermore, the disruption of discrimination was limited to closely related molecules, as chemogenetic silencing of cholinergic neurons did not affect discrimination of less similar odor pairs. Thus, ChAT-hM4Di mice injected with CNO displayed normal habituation/dishabituation for ethyl esters that differ by two carbons (Fig. 5*C*; C6, 3.5 ± 0.5 s vs C8, 7.8 ± 1.0 s, $p < 0.02$). Importantly, odor detection threshold for esters was not different between control and CNO-treated hM4Di mice (investigation time C7, 1:30,000, control 4.3 ± 0.5 s, CNO 3.7 ± 0.8 s; 1:40,000, control 0.6 ± 0.5 s, CNO 0.1 ± 0.8 s; see Materials and Methods). Together, these results indicate that transiently inhibiting HDB cholinergic neurons does not disrupt odor detection threshold but impairs discrimination of structurally similar odors.

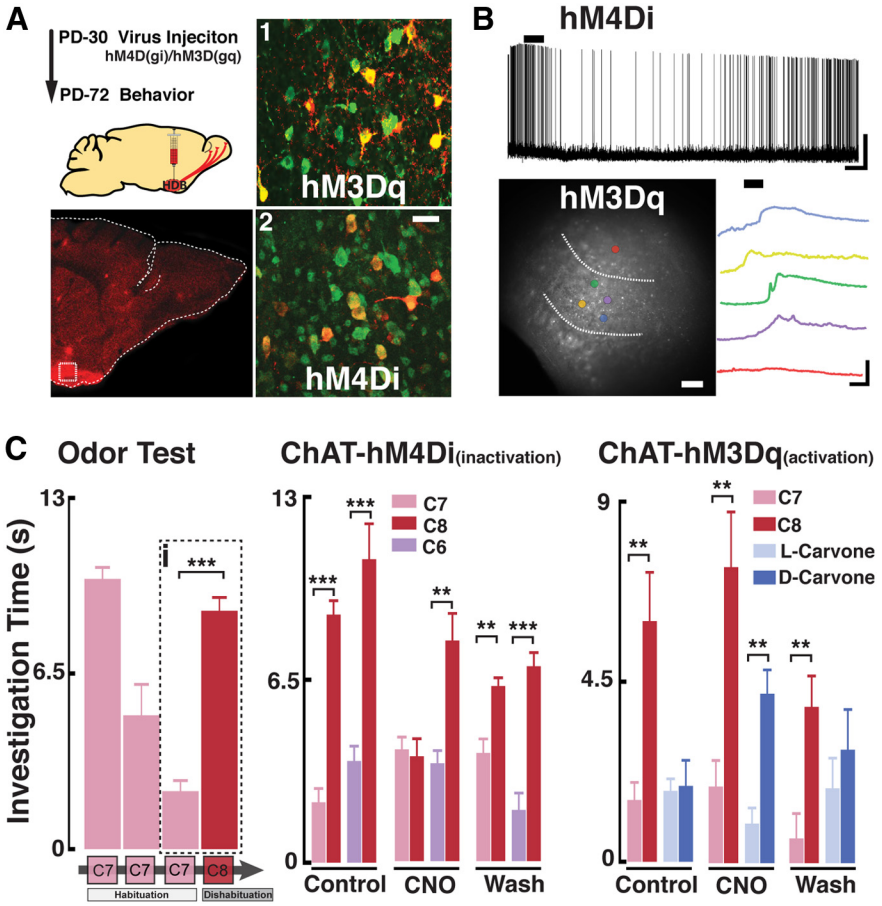

Figure 5. *In vivo* modification of HDB cholinergic neuron activity affects natural odor discrimination. ***A***, Top left, Schematic diagram for the virus injection and behavioral testing schedule. Bottom left, Confocal image of a sagittal section of the OB from a ChAT-Cre mouse expressing hM4Di (red, mCherry) in the HDB. Dotted box represents the region shown on the right pictures (***1***,***2***). ***A1***, ***A2***, Magnified HDB sections immunostained for ChAT (green) and mCherry (red) showing colocalization (yellow) with hM3Dq (***1***) and hM4Di (***2***). Scale bar, 25 μm. ***B***, Top, Recording from an HDB neuron expressing the hM4Di DREADD in the presence of iGluR blockers (APV 100 μM, CNQX 10 μM) and GABAzine (5 μM). Application of CNO (5 μM) produced a hyperpolarization in this cell ($V_m = -54$ mV). Calibration: 20 mV, 1 min. Bottom left, HDB neurons expressing the hM3Dq DREADD, loaded with the calcium dye Fluo-4. Dotted lines outline the HDB. Colored circles represent selected cells within the HDB (yellow, green, blue, and purple) responding to CNO. Red circle represents a cell outside the HDB. Bottom right, Optical recording traces color-coded to the cells shown on the left; cells in the HDB show an increase in calcium signal in the presence of CNO (5 μM). Calibration: 10% $\Delta F/F_0$, 2 min. ***C***, Left, Habituation/dishabituation protocol used to test natural discrimination of odors. Mice presented with the same odor (i.e., ethyl heptanoate, C7, pink) three times show a decrease in investigation time (habituation). On the fourth trial, a novel odor (i.e., ethyl octanoate, C8, red) is presented and investigation time increases (dishabituation). The dotted box (***i***) highlights the quantification of habituation/dishabituation for this odor set (C7/C8), which is used to determine the discrimination of odors pairs in the middle and right graphs. Middle, ChAT-hM4Di mice were tested for natural discrimination of the C7/C8 (pink/red) and C6/C8 (purple/red) odor pairs (ethyl hexanoate, C6, purple). Odor discrimination was assessed before CNO injection (Control, PBS injected), CNO injection (CNO), and 5 h after CNO (Wash). Right, ChAT-hM3Dq mice were similarly tested for olfactory discrimination with the C7/C8 odor pair and carvone isomers: dark blue represents L-carvone; light blue represents D-carvone. $^{**}p < 0.02$. $^{***}p < 0.01$.

To determine whether chemogenetic enhancement of ACh produces the opposite effect in odor discrimination, we tested the ChAT-hM3Dq mice against odor pairs that these mice naturally fail to discriminate. Like wild-type mice (data not shown), ChAT-hM3Dq mice injected with saline fail to discriminate the L-

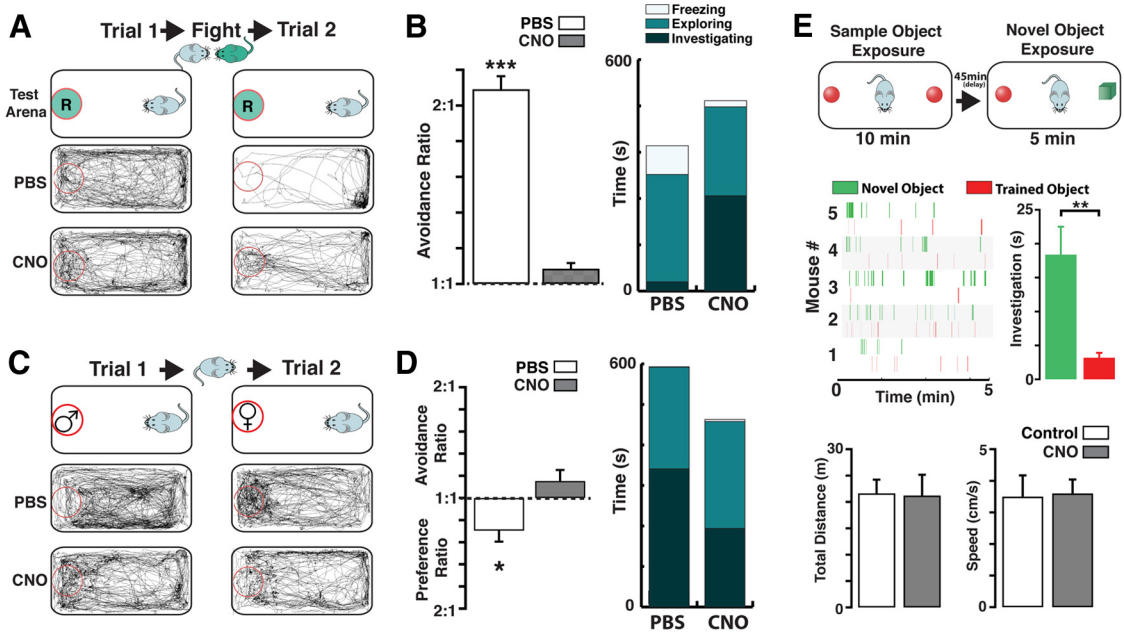

Figure 6. Chemogenetic silencing of cholinergic neurons disrupts investigation of social odors. ***A***, Top, Schematic illustration of the behavior paradigm used for the aggression-induced olfactory avoidance (see Materials and Methods). Before the aggressive encounter, a ChAT-hM4Di intruder (light blue) is placed in a neutral environment (Trial 1, 15 min), containing a dish with the soiled bedding from a resident (green circle marked "R"). Following the aggressive encounter, in which the intruder loses the fight, the same odor presentation is repeated (Trial 2, 15 min). Bottom, Movement trajectories during Trials 1 and 2, before the fight mice injected with PBS show no preference for a particular region of the neutral environment (left). After the fight, the mice spend most of the time avoiding the dish containing the resident's bedding (right). Following the fight, mice injected with CNO in the presence of the resident's bedding show no avoidance. ***B***, Left, The avoidance ratio is significantly larger for the PBS-treated mice (white bar) compared with the CNO group (gray bar). Right, Stacked bar graph represents the average freezing (white), exploration (light green), and investigating (dark green) times, after fight (Trial 2) for PBS and CNO group. ***C***, Top, Schematic illustration for the assessment of female odor preference (see Materials and Methods). During the first trial (Trial 1, 15 min), a ChAT-hM4Di male mouse is presented with a dish containing male-soiled bedding (red circle marked "♂"), whereas in the second trial (Trial 2, 15 min), the mouse is presented with a dish containing a female's soiled bedding (red circle marked "♀"). Bottom, Movement trajectories during Trials 1 and 2. In the presence of male bedding, mice injected with PBS navigate throughout the neutral environment indiscriminately (left). In the presence of female bedding, males spend significantly more time investigating the dish. In mice injected with CNO, the movement trajectories show decreased preference for a female's bedding. ***D***, Left, The preference ratio is significant in the PBS-treated mice (white bar), whereas the CNO-treated mice show no preference, instead show a small but nonsignificant avoidance ratio (gray). Right, Stacked bar graph represents the average time spent by mice exhibiting freezing (white), exploration (light green), and investigation (dark green) behaviors during Trial 2 for the PBS and CNO groups. ***E***, Top, Schematic illustration for the novel object recognition task. The trained object (red) consisted of a marble while the novel object was a cube (green, see Materials and Methods). Middle, Raster plots for the investigation events of the novel object in different ChAT-hM4Di mice injected with CNO. The mice spend a significant amount of time investigating the novel object. Bottom, The exploratory distance (left) and the average speed during the task is not affected by CNO. $*p < 0.05$; $**p < 0.02$; $***p < 0.01$.

and D-carvone isomers (Fig. 5*C*; L-carvone, 2.4 ± 0.4 s; D-carvone, 2.5 ± 0.9 s, $n = 4$, $p = 0.84$), or the α- and β-pinene pair (α, 2.1 ± 0.6 vs β, 1.8 ± 0.5 s, $n = 4$, $p = 0.66$, data not shown). Interestingly, after CNO injection, ChAT-hM3Dq mice were now able to discriminate the carvone isomers (Fig. 5*C*; L-carvone, 1.3 ± 0.5 s vs D-carvone, 5.6 ± 0.8 s, $p < 0.02$). Similarly, the investigation time during dishabituation also increased for the α-β pinene pair, although within our limited sample this increase was not significant (α 2.4 ± 0.5 vs β 4.3 ± 0.5, $n = 4$, $p < 0.07$; data not shown). As expected, ChAT-hM3Dq mice injected with CNO were still able to discriminate the C7/C8 pair (C7, 2.1 ± 0.7 vs C8, 7.1 ± 0.8 s, $n = 4$, $p < 0.02$). Interestingly, similar to the hM4Di mice, odor detection threshold was not affected in hM3Dq mice after CNO (investigation time C7, 1:30,000, control 4.3 ± 0.5 s, CNO 3.9 ± 0.2 s; 1:40,000, control 0.6 ± 0.5 s, hM3Dq 0.8 ± 0.4 s). These results indicate that chemogenetic manipulation of cholinergic tone in the MOB produces a reliable and reversible outcome on the natural discrimination of odors. Surprisingly, however, odor detection threshold is not affected by these manipulations.

Chemogenetic silencing of HDB cholinergic neurons disrupts investigation of social odors

The dense innervation of the AOB by HDB neurons and the neuromodulation of this circuit by ACh predict an important regulation of behaviors signaled through the VNS by the cholinergic system; however, at present, this possibility remains unknown. We therefore examined the natural investigation of semiochemicals in male ChAT-hM4Di mice in the context of aggressive and sexual behaviors, which are known to rely on VNS signaling (Chamero et al., 2007). Overall, the motor behavior, characterized by the total exploratory distance and speed, was not different between PBS and CNO injected ChAT-hM4Di mice (exploratory distance, PBS vs CNO, 5232 ± 532 vs 4451 ± 676 cm; speed, cm/s, 5.8 ± 0.6 vs 5.0 ± 0.8, $n = 4$, $p = 0.39$). These results indicate that, under experimental conditions, chemogenetic inhibition of HDB cholinergic neurons does not disrupt motor behavior.

Next, we assessed male avoidance to the odor of a dominant male following an aggressive encounter using the resident-intruder paradigm (Koolhaas et al., 2013) (see Materials and Methods). Before the aggressive encounter, naive ChAT-hM4Di intruder males injected with PBS (control) or CNO showed neither preference nor avoidance for the bedding soiled with odors of the resident (Trial 1, 15 min), spending a similar average distance from the dish (D.D.) containing the bedding (Fig. 6*A*; D.D., PBS vs CNO, 13.1 ± 1.5 vs 13.0 ± 1.7 cm, $n = 4$, $p = 0.9$). However, after the aggressive encounter (in which the resident defeats the intruder), intruders injected with PBS exhibited strong avoidance toward the resident's soiled bedding (Fig. 6*B*;

D.D., PBS Trial 1 vs Trial 2, 13.1 ± 1.5 vs 27.4 ± 0.7 cm, $n = 4$, $p < 0.01$; ratio 2.1 ± 0.2). It should be noted that in this assay the avoidance behavior in the intruder is elicited only by the odor of the resident encountered during the fight. Thus, defeated mice presented with the soiled bedding of a different resident (unknown to the intruder) do not exhibit this avoidance behavior (D.D. Trial 1 vs Trial 2, 14.3 ± 0.5 vs 15.2 ± 0.7 cm, $n = 4$, $p = 0.42$), indicating that the avoidance does not generalize to odor of other males nor that it results from an unspecific change in behavior after fight. Importantly, intruders injected with CNO do not show avoidance for the resident's soiled bedding after the fight (Fig. 6*A*; D.D., CNO Trial 1 vs Trial 2, 13.0 ± 1.7 vs 14.2 ± 3.6 cm, $n = 4$, $p = 0.67$; ratio 1.09 ± 0.03). Additionally, in contrast to PBS-injected mice after the aggression encounter, the CNO-injected group spent more time investigating the Petri dish (Fig. 6*B*, right, investigation time, PBS 20.4 ± 8.1 vs CNO 206 ± 31 s, $n = 4$, $p < 0.01$). However, the time spent displaying exploratory behaviors (see Materials and Methods) was not different between the two groups after the fight (Fig. 6*B*, right, exploration time, PBS, 232 ± 32 vs CNO, 192 ± 26 s, $n = 4$, $p = 0.50$). We also observed a significant reduction in grooming and freezing in mice injected with CNO (grooming time, PBS vs CNO, 351 ± 33 vs 214 ± 22 s, $p < 0.02$; freezing time, 62.9 ± 18.1 vs 13.3 ± 5.2 s, $n = 4$, $p < 0.04$), reflecting less anxiety-related behaviors after fight in the defeated mice.

In addition to aggressive behaviors, the VNS plays an important role in the detection and processing of semiochemicals that trigger sexual behaviors (Stowers et al., 2013). Therefore, we assessed the investigative behavior of naive ChAT-hM4Di males toward bedding containing female odors. As shown in Figure 6*C*, under control conditions males showed a significant preference for female-soiled bedding compared with nonspecific male-soiled bedding (Fig. 6*C*; D.D., male vs female-soiled bedding, 17.5 ± 0.5 vs 12.5 ± 1.7 cm, $n = 4$, $p < 0.03$; ratio −1.29 ± 0.13). However, ChAT-hM4Di males injected with CNO no longer showed preference (or avoidance) for female-soiled bedding compared with control males (D.D., CNO, 13.3 ± 1.1 vs 14.6 ± 1.2 cm, $n = 4$, $p = 0.40$, ratio 1.09 ± 0.09). Accordingly, we found that the CNO injected mice spent less time investigating the dish (investigation time PBS vs CNO, 366 ± 36 vs 194 ± 15 s, $n = 4$, $p < 0.01$). However, the overall exploring time, grooming, and freezing were not different in the CNO-injected ChAT-hM4Di males (Fig. 6*D*, right, grooming time PBS vs CNO, 11.9 ± 5.1 vs 17.1 ± 11.9 s, $p = 0.65$; freezing time, 2.85 ± 0.12 vs 4.67 ± 1.22 s, $n = 4$, $p = 0.3$; exploring time, 251 ± 6 vs 264 ± 11 s, $n = 4$, $p = 0.43$). Additionally, CNO injection in ChAT-hM4Di males does not affect the investigation of other male's bedding (D.D., before CNO 17.5 ± 0.5 cm; after CNO, 16.2 ± 1.5 cm, $n = 4$, $p = 0.44$). Together these results suggest that a reduction of cholinergic tone also disrupts the natural preference of male mice for female odors.

Last, we wondered whether inhibition of cholinergic function in the ChAT-hM4Di mice could also interfere with a nonolfactory task. To this extent, we used a novel object-recognition task (Bevins and Besheer, 2006). As shown Figure 6*E* (bottom), ChAT-hM4Di mice injected with CNO do not show difference in exploratory distance (Control vs CNO, 2164 ± 259 vs 2123 ± 393 cm, $p = 0.93$, $n = 5$) or average speed (Control vs CNO, 3.5 ± 0.67 vs 3.6 ± 0.44 cm/s, $p = 0.95$, $n = 5$) during the task (see Materials and Methods). Importantly, novel object recognition was not disrupted by the CNO injection (Fig. 6*E*, top). During the task, ChAT-hM4Di CNO-treated mice spend >80% of the time investigating the new object (novel object, 18.6 ± 4.6 s vs trained object 3.2 ± 0.7 s, $p < 0.01$, $n = 5$). Thus, under our experimental conditions, the behavioral deficits in CNO-treated ChAT-hM4Di mice are not widespread.

Discussion

The MOB and AOB have a remarkably similar neural circuit, including prominent neuromodulatory regulation by ACh. Despite this conserved circuitry, we found striking differences in muscarinic cholinergic modulation between the MOB and AOB. Endogenous release of ACh elicited a consistent depolarization of MCs in the AOB but elicited a hyperpolarization in MOB MCs. Similarly, the predominant muscarinic effect on GCs is hyperpolarization in the MOB, but depolarization in the AOB. The pharmacological profile of the inhibitory response in MOB MCs and GCs, together with its persistence in the *M1/M3*$^{-/-}$ mice, indicated the participation of M2 mAChRs. Throughout the OB, M1-like (M1, M3, and M5) and M2-like (M2 and M4) receptors exhibit abundant expression (Le Jeune et al., 1996; Hamilton and Hayar, 2007), and these receptors produce different cellular effects (Wess et al., 2007). Thus, our studies are the first to show a physiological role for M2 receptors in the OB.

The M2-mediated inhibition in MOB MCs described here agrees with previous *in vivo* studies showing inhibitory effects in MCs by ACh (Bloom et al., 1964; Nickell and Shipley, 1988). In addition, in agreement with the M2-mediated inhibition of GCs, nonselective cholinergic agonists decreased the frequency of spontaneous action potentials in MOB GCs (Castillo et al., 1999). On the other hand, M1 mAChR activation increased the excitability in MOB and AOB GCs, including depolarization and the activation of an sAPD, leading to an increase of GABA release onto MCs (Pressler et al., 2007; Ghatpande and Gelperin, 2009; Smith and Araneda, 2010). Together, our results provide the first evidence that neuronal components of the AOB and MOB are regulated in opposing fashion by ACh, recruiting the activation of M2 and M1 mAChRs to produce inhibitory and excitatory effects, respectively.

GCs play an important role in lateral inhibition and network oscillations in the MOB (Shepherd et al., 2007). The inhibitory and excitatory components of muscarinic modulation in MOB GCs suggest that the overall inhibition of MCs in the presence of ACh will greatly depend on the level of activity in the circuit (Li and Cleland, 2013). We propose that, at subthreshold levels of activation in MOB GCs, the M2-mediated hyperpolarization is the predominant effect of ACh, reducing the inhibitory drive onto GC-MC synapses. However, in the presence of strong excitatory input onto GCs (i.e., from excited MCs), the M1-mediated activation of the sADP will prevail, prolonging the activation of GCs (Pressler et al., 2007). In turn, activation of M1-mAChRs is always excitatory in AOB GCs, suggesting that GCs contribute differently to the overall response of MCs. One possibility is that ACh produces a more generalized increase in excitability in the AOB, not to enhance odor discrimination, but rather to facilitate the integration of pheromonal signals. In this case, a reduction in ACh levels will disrupt signal integration and thus behavior (see below).

It is noteworthy that MCs, but not GCs, exhibit a nicotinic excitatory response in the AOB and MOB (Castillo et al., 1999; Smith and Araneda, 2010; D'Souza and Vijayaraghavan, 2012), yet optogenetic stimulation indicated a predominant muscarinic response in MCs. One possibility is that our stimulation protocol induces fast desensitization of nAChRs. However, a similar hyperpolarization of MOB MCs by optogenetic stimulation of HDB neurons was recently reported (Ma and Luo, 2012). Yet other

studies show excitation of MCs in the MOB (Kunze et al., 1991; Zhan et al., 2013; Rothermel et al., 2014). At this time, the reason for these discrepancies remains unknown. One possibility is that the location used for the optical stimulation (i.e., superficial OB, or OB vs HDB) or actions on multiple targets may have contributed to these differences (Devore et al., 2014). For example, the distribution of cholinergic fibers in the GC layer and the muscarinic effects in GCs reported here and elsewhere (Pressler et al., 2007; Smith and Araneda, 2010) suggest that *in vivo* optogenetic stimulation will be affected by the degree GCs are stimulated (see below).

Modulation of gain is a key mechanism for the proper integration and processing of sensory signals, relying on a synaptic network that conducts scaling and thresholding functions (McKenna et al., 1988; Metherate et al., 1988; Pinto et al., 2013). Interestingly, endogenous release of ACh had a different effect on the input–output relationship of MCs in the AOB and MOB, showing a net effect on gain in MCs of the MOB, but not in the AOB. Stimulation of superficial layers of the MOB indicated that ACh increases the threshold for sensory input by exciting MCs (Rothermel et al., 2014). Furthermore, in the MOB, ACh has been shown to modulate external tufted and periglomerular cells (Pignatelli and Belluzzi, 2008; D'Souza et al., 2013; Liu et al., 2015). These cells are part of the glomerular network involved in processing incoming odor signals (Shao et al., 2009; Gire et al., 2012). When the HDB is directly activated, which should achieve a widespread activation of cholinergic fibers, the effect on MOB MCs becomes inhibitory, which is a noteworthy result (Ma and Luo, 2012; Rothermel et al., 2014). Thus, it is possible that glomerular circuit excitation, most likely nicotinic, could modulate MC output despite the fact that the overall effect of ACh is inhibitory in MOB MCs. Cholinergic fibers and other cholinergic markers appeared excluded from the AOB GL, suggesting that ACh could have a lesser role in regulating sensory input at this level. Although we cannot rule out the possibility that ACh could access the GL through volume transmission (Sarter et al., 2009), it is possible that the lack of innervation on the GL underlies differences in processing. For example, chemosensory representation in the GL of the MOB shows tunotopy, whereas in the AOB the representation is based on the phenotypic identity of social odors (Ma et al., 2012; Hammen et al., 2014). In addition, in the AOB, information from several subclasses of receptor types is integrated into a single MC at the level of the GL (Wagner et al., 2006). Therefore, MCs in the AOB are poised to integrate sensory information from widespread odor sources, whereas its counterparts in the MOB may serve a more analytical role (Dulac and Wagner, 2006).

Detection and processing of semiochemicals by the VNS are fundamental for several social interactions, predominantly sexual and aggressive behaviors (Halpern and Martínez-Marcos, 2003; Brennan and Zufall, 2006). Neuromodulation plays a critical role in behaviors that require signaling through the VNS (Brennan and Keverne, 1997; Brennan and Kendrick, 2006). Here, silencing the activity of HDB cholinergic neurons disrupted odor discrimination while transiently enhancing the activity of these neurons produced a dramatic improvement in the natural discrimination of odors. Previous pharmacological studies reached a similar conclusion (Mandairon et al., 2006), indicating that the chemogenetic approach, which replicates *in vivo* modifications of synaptic activity and physiological release of ACh, provides a reliable platform to assess the role of cholinergic modulation on VNS function. Using this approach, we found that silencing HDB cholinergic neurons impaired the ability of the defeated mouse to recognize the aggressor's odor and disrupted the investigation of female odors by males. Previous studies have shown that the cues necessary for eliciting these behaviors are mediated by the VNS (Chamero et al., 2007; Haga et al., 2010; Haga-Yamanaka et al., 2014). Together, these results indicate that reducing cholinergic tone has deleterious effects on odor-triggered behaviors that rely on VNS signaling. Interestingly, habituation to social odors was reduced by nonselective pharmacological manipulation of the cholinergic system (Winslow and Camacho, 1995); however, our selective chemogenetic silencing of the HDB had no effect in habituation to odors. Our experiments do not rule out the participation of other brain regions targeted by HDB cholinergic neurons, such as the piriform and entorhinal cortices (Zaborszky et al., 2012). However, we found that chemogenetic inhibition of HDB neurons did not impair "recognition memory" (Bevins and Besheer, 2006). Previous studies have shown that this paradigm is affected by damage of forebrain cholinergic neurons (Kornecook et al., 1999; Paban et al., 2005). Conversely, recent studies suggest that MOB and VNS play complementary roles in processing social odors; therefore, the contribution of cholinergic projections in the MOS could also contribute to the observed effects (Mucignat-Caretta et al., 2012; Korzan et al., 2013; Baum and Cherry, 2015). Nevertheless, our data support a cholinergic neuromodulatory role for social behaviors that signal through the VNS; further studies should elucidate the specific contributions of the MOS and VNS in social odor investigations.

In conclusion, cholinergic modulation in the OB has an important role in the olfactory system; it facilitates odor discrimination and investigation of socially relevant semiochemicals. Despite the conserved nature of the neural circuits that process these sensory cues in the MOB and AOB, cholinergic modulation of these circuits exhibits a marked difference, anatomically and physiologically. It is noteworthy that noradrenaline, another neuromodulator that regulates OB circuits, also shows significant differences in the cellular actions in these circuits (Nai et al., 2009; Zimnik et al., 2013). Thus, these neuromodulatory differences highlight the specialized function of these two parallel pathways in regard to stimulus composition and the behavioral output they trigger. Our results highlight the emerging view on the function of neuromodulation; neural circuits, in the presence of multiple neuromodulators, can produce the same output using several different mechanisms (Marder, 2012). Future studies will examine whether the neuromodulation of upstream components in these pathways also exhibits differential regulation by the cholinergic system.

References

Armbruster BN, Li X, Pausch MH, Herlitze S, Roth BL (2007) Evolving the lock to fit the key to create a family of G protein-coupled receptors potently activated by an inert ligand. Proc Natl Acad Sci U S A 104:5163–5168. CrossRef Medline

Baum MJ, Cherry JA (2015) Processing by the main olfactory system of chemosignals that facilitate mammalian reproduction. Horm Behav 68:53–64. CrossRef Medline

Bevins RA, Besheer J (2006) Object recognition in rats and mice: a one-trial non-matching-to-sample learning task to study "recognition memory." Nat Protoc 1:1306–1311. CrossRef

Bloom FE, Costa E, Salmoiraghi GC (1964) Analysis of individual rabbit olfactory bulb neuron responses to microelectrophoresis of acetylcholine norepinephrine + serotonin synergists + antagonists. J Pharmacol Exp Ther 146:16–23. Medline

Brennan PA, Kendrick KM (2006) Mammalian social odours: attraction and individual recognition. Philos Trans R Soc Lond B Biol Sci 361:2061–2078. CrossRef Medline

Brennan PA, Keverne EB (1997) Neural mechanisms of mammalian olfactory learning. Prog Neurobiol 51:457–481. CrossRef Medline

Brennan PA, Zufall F (2006) Pheromonal communication in vertebrates. Nature 444:308–315. CrossRef Medline

Castillo PE, Carleton A, Vincent JD, Lledo PM (1999) Multiple and opposing roles of cholinergic transmission in the main olfactory bulb. J Neurosci 19:9180–9191. Medline

Chamero P, Marton TF, Logan DW, Flanagan K, Cruz JR, Saghatelian A, Cravatt BF, Stowers L (2007) Identification of protein pheromones that promote aggressive behaviour. Nature 450:899–902. CrossRef Medline

Chance FS, Abbott LF, Reyes AD (2002) Gain modulation from background synaptic input. Neuron 35:773–782. CrossRef Medline

Chapuis J, Wilson DA (2013) Cholinergic modulation of olfactory pattern separation. Neurosci Lett 545:50–53. CrossRef Medline

Chaudhury D, Escanilla O, Linster C (2009) Bulbar acetylcholine enhances neural and perceptual odor discrimination. J Neurosci 29:52–60. CrossRef Medline

Devore S, de Almeida L, Linster C (2014) Distinct roles of bulbar muscarinic and nicotinic receptors in olfactory discrimination learning. J Neurosci 34:11244–11260. CrossRef Medline

Doty RL, Bagla R, Kim N (1999) Physostigmine enhances performance on an odor mixture discrimination test. Physiol Behav 65:801–804. Medline

D'Souza RD, Vijayaraghavan S (2012) Nicotinic receptor-mediated filtering of mitral cell responses to olfactory nerve inputs involves the alpha3beta4 subtype. J Neurosci 32:3261–3266. CrossRef Medline

D'Souza RD, Vijayaraghavan S (2014) Paying attention to smell: cholinergic signaling in the olfactory bulb. Front Synaptic Neurosci 6:21. CrossRef Medline

D'Souza RD, Parsa PV, Vijayaraghavan S (2013) Nicotinic receptors modulate olfactory bulb external tufted cells via an excitation-dependent inhibitory mechanism. J Neurophysiol 110:1544–1553. CrossRef Medline

Dulac C, Wagner S (2006) Genetic analysis of brain circuits underlying pheromone signaling. Annu Rev Genet 40:449–467. CrossRef Medline

Fournier GN, Semba K, Rasmusson DD (2004) Modality- and region-specific acetylcholine release in the rat neocortex. Neuroscience 126:257–262. CrossRef Medline

Galán RF, Ermentrout GB, Urban NN (2008) Optimal time scale for spike-time reliability: theory, simulations, and experiments. J Neurophysiol 99:277–283. CrossRef Medline

Gautam D, Heard TS, Cui Y, Miller G, Bloodworth L, Wess J (2004) Cholinergic stimulation of salivary secretion studied with M1 and M3 muscarinic receptor single- and double-knockout mice. Mol Pharmacol 66:260–267. CrossRef Medline

Ghatpande AS, Gelperin A (2009) Presynaptic muscarinic receptors enhance glutamate release at the mitral/tufted to granule cell dendrodendritic synapse in the rat main olfactory bulb. J Neurophysiol 101:2052–2061. CrossRef Medline

Ghatpande AS, Sivaraaman K, Vijayaraghavan S (2006) Store calcium mediates cholinergic effects on mIPSCs in the rat main olfactory bulb. J Neurophysiol 95:1345–1355. CrossRef Medline

Gire DH, Franks KM, Zak JD, Tanaka KF, Whitesell JD, Mulligan AA, Hen R, Schoppa NE (2012) Mitral cells in the olfactory bulb are mainly excited through a multistep signaling path. J Neurosci 32:2964–2975. CrossRef Medline

Gire DH, Restrepo D, Sejnowski TJ, Greer C, De Carlos JA, Lopez-Mascaraque L (2013) Temporal processing in the olfactory system: can we see a smell? Neuron 78:416–432. CrossRef Medline

Haga S, Hattori T, Sato T, Sato K, Matsuda S, Kobayakawa R, Sakano H, Yoshihara Y, Kikusui T, Touhara K (2010) The male mouse pheromone ESP1 enhances female sexual receptive behaviour through a specific vomeronasal receptor. Nature 466:118–122. CrossRef Medline

Haga-Yamanaka S, Ma L, He J, Qiu Q, Lavis LD, Looger LL, Yu CR (2014) Integrated action of pheromone signals in promoting courtship behavior in male mice. Elife 3:e03025. CrossRef Medline

Halpern M, Martínez-Marcos A (2003) Structure and function of the vomeronasal system: an update. Prog Neurobiol 70:245–318. CrossRef Medline

Hamilton EM, Hayar A (2007) Neurochemistry of the main olfactory system. In: Handbook of neurochemistry and molecular neurobiology, pp 137–204. New York: Springer.

Hammen GF, Turaga D, Holy TE, Meeks JP (2014) Functional organization of glomerular maps in the mouse accessory olfactory bulb. Nat Neurosci 17:953–961. CrossRef Medline

Hellier JL, Arevalo NL, Smith L, Xiong KN, Restrepo D (2012) α7-Nicotinic acetylcholine receptor: role in early odor learning preference in mice. PLoS One 7:e35251. CrossRef Medline

Kay LM, Sherman SM (2007) An argument for an olfactory thalamus. Trends Neurosci 30:47–53. CrossRef Medline

Koolhaas JM, Coppens CM, de Boer SF, Buwalda B, Meerlo P, Timmermans PJ (2013) The resident-intruder paradigm: a standardized test for aggression, violence and social stress. J Vis Exp e4367.

Kornecook TJ, Kippin TE, Pinel JP (1999) Basal forebrain damage and object-recognition in rats. Behav Brain Res 98:67–76. CrossRef Medline

Korzan WJ, Freamat M, Johnson AG, Cherry JA, Baum MJ (2013) Either main or accessory olfactory system signaling can mediate the rewarding effects of estrous female chemosignals in sexually naive male mice. Behav Neurosci 127:755–762. CrossRef Medline

Krosnowski K, Ashby S, Sathyanesan A, Luo W, Ogura T, Lin W (2012) Diverse populations of intrinsic cholinergic interneurons in the mouse olfactory bulb. Neuroscience 213:161–178. CrossRef Medline

Kunze WA, Shafton AD, Kemm RE, McKenzie JS (1991) Effect of stimulating the nucleus of the horizontal limb of the diagonal band on single unit-activity in the olfactory-bulb. Neuroscience 40:21–27. CrossRef Medline

Larriva-Sahd J (2008) The accessory olfactory bulb in the adult rat: a cytological study of its cell types, neuropil, neuronal modules, and interactions with the main olfactory system. J Comp Neurol 510:309–350. CrossRef Medline

Lee MG, Hassani OK, Alonso A, Jones BE (2005) Cholinergic basal forebrain neurons burst with theta during waking and paradoxical sleep. J Neurosci 25:4365–4369. CrossRef Medline

Le Jeune H, Aubert I, Jourdan F, Quirion R (1996) Developmental profiles of various cholinergic markers in the rat main olfactory bulb using quantitative autoradiography. J Comp Neurol 373:433–450. CrossRef Medline

Li G, Cleland TA (2013) A two-layer biophysical model of cholinergic neuromodulation in olfactory bulb. J Neurosci 33:3037–3058. CrossRef Medline

Linster C, Cleland TA (2002) Cholinergic modulation of sensory representations in the olfactory bulb. Neural Netw 15:709–717. CrossRef Medline

Linster C, Fontanini A (2014) Functional neuromodulation of chemosensation in vertebrates. Curr Opin Neurobiol 29C:82–87. CrossRef Medline

Liu S, Shao Z, Puche A, Wachowiak M, Rothermel M, Shipley MT (2015) Muscarinic receptors modulate dendrodendritic inhibitory synapses to sculpt glomerular output. J Neurosci 35:5680–5692. CrossRef Medline

Ma L, Qiu Q, Gradwohl S, Scott A, Yu EQ, Alexander R, Wiegraebe W, Yu CR (2012) Distributed representation of chemical features and tunotopic organization of glomeruli in the mouse olfactory bulb. Proc Natl Acad Sci U S A 109:5481–5486. CrossRef Medline

Ma M, Luo M (2012) Optogenetic activation of basal forebrain cholinergic neurons modulates neuronal excitability and sensory responses in the main olfactory bulb. J Neurosci 32:10105–10116. CrossRef Medline

Mandairon N, Ferretti CJ, Stack CM, Rubin DB, Cleland TA, Linster C (2006) Cholinergic modulation in the olfactory bulb influences spontaneous olfactory discrimination in adult rats. Eur J Neurosci 24:3234–3244. CrossRef Medline

Manns ID, Alonso A, Jones BE (2000) Discharge properties of juxtacellularly labeled and immunohistochemically identified cholinergic basal forebrain neurons recorded in association with the electroencephalogram in anesthetized rats. J Neurosci 20:1505–1518. Medline

Marder E (2012) Neuromodulation of neuronal circuits: back to the future. Neuron 76:1–11. CrossRef Medline

Marguet SL, Harris KD (2011) State-dependent representation of amplitude-modulated noise stimuli in rat auditory cortex. J Neurosci 31:6414–6420. CrossRef Medline

McKenna TM, Ashe JH, Hui GK, Weinberger NM (1988) Muscarinic agonists modulate spontaneous and evoked unit discharge in auditory cortex of cat. Synapse 2:54–68. CrossRef Medline

Metherate R, Tremblay N, Dykes RW (1988) The effects of acetylcholine on response properties of cat somatosensory cortical neurons. J Neurophysiol 59:1231–1252. Medline

Mucignat-Caretta C, Redaelli M, Caretta A (2012) One nose, one brain: contribution of the main and accessory olfactory system to chemosensation. Front Neuroanat 6:46. CrossRef Medline

Nai Q, Dong HW, Hayar A, Linster C, Ennis M (2009) Noradrenergic regulation of GABAergic inhibition of main olfactory bulb mitral cells varies

as a function of concentration and receptor subtype. J Neurophysiol 101: 2472–2484. CrossRef Medline

Nickell WT, Shipley MT (1988) Neurophysiology of magnocellular forebrain inputs to the olfactory bulb in the rat: frequency potentiation of field potentials and inhibition of output neurons. J Neurosci 8:4492–4502. Medline

Niell CM, Stryker MP (2010) Modulation of visual responses by behavioral state in mouse visual cortex. Neuron 65:472–479. CrossRef Medline

Nunez-Parra A, Maurer RK, Krahe K, Smith RS, Araneda RC (2013) Disruption of centrifugal inhibition to olfactory bulb granule cells impairs olfactory discrimination. Proc Natl Acad Sci U S A 110:14777–14782. CrossRef Medline

Paban V, Chambon C, Jaffard M, Alescio-Lautier B (2005) Behavioral effects of basal forebrain cholinergic lesions in young adult and aging rats. Behav Neurosci 119:933–945. CrossRef Medline

Padmanabhan K, Urban NN (2010) Intrinsic biophysical diversity decorrelates neuronal firing while increasing information content. Nat Neurosci 13:1276–1282. CrossRef Medline

Parikh V, Sarter M (2008) Cholinergic mediation of attention: contributions of phasic and tonic increases in prefrontal cholinergic activity. Ann N Y Acad Sci 1129:225–235. CrossRef Medline

Petersen CC (2014) Cortical control of whisker movement. Annu Rev Neurosci 37:183–203. CrossRef Medline

Pignatelli A, Belluzzi O (2008) Cholinergic modulation of dopaminergic neurons in the mouse olfactory bulb. Chem Senses 33:331–338. CrossRef Medline

Pinto L, Goard MJ, Estandian D, Xu M, Kwan AC, Lee SH, Harrison TC, Feng G, Dan Y (2013) Fast modulation of visual perception by basal forebrain cholinergic neurons. Nat Neurosci 16:1857–1863. CrossRef Medline

Pressler RT, Inoue T, Strowbridge BW (2007) Muscarinic receptor activation modulates granule cell excitability and potentiates inhibition onto mitral cells in the rat olfactory bulb. J Neurosci 27:10969–10981. CrossRef Medline

Rossi J, Balthasar N, Olson D, Scott M, Berglund E, Lee CE, Choi MJ, Lauzon D, Lowell BB, Elmquist JK (2011) Melanocortin-4 receptors expressed by cholinergic neurons regulate energy balance and glucose homeostasis. Cell Metab 13:195–204. CrossRef Medline

Rothermel M, Carey RM, Puche A, Shipley MT, Wachowiak M (2014) Cholinergic inputs from basal forebrain add an excitatory bias to odor coding in the olfactory bulb. J Neurosci 34:4654–4664. CrossRef Medline

Salcedo E, Tran T, Ly X, Lopez R, Barbica C, Restrepo D, Vijayaraghavan S (2011) Activity-dependent changes in cholinergic innervation of the mouse olfactory bulb. PLoS One 6:e25441. CrossRef Medline

Sarter M, Parikh V, Howe WM (2009) Phasic acetylcholine release and the volume transmission hypothesis: time to move on. Nat Rev Neurosci 10:383–390. CrossRef Medline

Shao Z, Puche AC, Kiyokage E, Szabo G, Shipley MT (2009) Two GABAergic intraglomerular circuits differentially regulate tonic and phasic presynaptic inhibition of olfactory nerve terminals. J Neurophysiol 101: 1988–2001. CrossRef Medline

Shepherd GM, Greer CA (1998) Olfactory bulb. In: The synaptic organization of the brain, Ed 4 (Shepherd GM, ed), pp 159–204. Oxford: Oxford University.

Shepherd GM, Chen WR, Willhite D, Migliore M, Greer CA (2007) The olfactory granule cell: from classical enigma to central role in olfactory processing. Brain Res Rev 55:373–382. CrossRef Medline

Shpak G, Zylbertal A, Wagner S (2014) Transient and sustained afterdepolarizations in accessory olfactory bulb mitral cells are mediated by distinct mechanisms that are differentially regulated by neuromodulators. Front Cell Neurosci 8:432. CrossRef Medline

Shusterman R, Smear MC, Koulakov AA, Rinberg D (2011) Precise olfactory responses tile the sniff cycle. Nat Neurosci 14:1039–1044. CrossRef Medline

Smith RS, Araneda RC (2010) Cholinergic modulation of neuronal excitability in the accessory olfactory bulb. J Neurophysiol 104:2963–2974. CrossRef Medline

Smith RS, Weitz CJ, Araneda RC (2009) Excitatory actions of noradrenaline and metabotropic glutamate receptor activation in granule cells of the accessory olfactory bulb. J Neurophysiol 102:1103–1114. CrossRef Medline

Sternson SM, Roth BL (2014) Chemogenetic tools to interrogate brain functions. Annu Rev Neurosci 37:387–407. CrossRef Medline

Stowers L, Cameron P, Keller JA (2013) Ominous odors: olfactory control of instinctive fear and aggression in mice. Curr Opin Neurobiol 23:339–345. CrossRef Medline

Wagner S, Gresser AL, Torello AT, Dulac C (2006) A multireceptor genetic approach uncovers an ordered integration of VNO sensory inputs in the accessory olfactory bulb. Neuron 50:697–709. CrossRef Medline

Wess J, Eglen RM, Gautam D (2007) Muscarinic acetylcholine receptors: mutant mice provide new insights for drug development. Nat Rev Drug Discov 6:721–733. CrossRef Medline

Wilson DA, Fletcher ML, Sullivan RM (2004) Acetylcholine and olfactory perceptual learning. Learn Mem 11:28–34. CrossRef Medline

Winslow JT, Camacho F (1995) Cholinergic modulation of a decrement in social investigation following repeated contacts between mice. Psychopharmacology (Berl) 121:164–172. CrossRef Medline

Zaborszky L, van den Pol A, Gyengesi E (2012) The basal forebrain cholinergic projection system in mice. Mouse Nerv Syst 684–718.

Zhan X, Yin P, Heinbockel T (2013) The basal forebrain modulates spontaneous activity of principal cells in the main olfactory bulb of anesthetized mice. Front Neural Circuits 7:148. CrossRef Medline

Zhao S, Ting JT, Atallah HE, Qiu L, Tan J, Gloss B, Augustine GJ, Deisseroth K, Luo M, Graybiel AM, Feng G (2011) Cell type-specific channelrhodopsin-2 transgenic mice for optogenetic dissection of neural circuitry function. Nat Methods 8:745–752. CrossRef Medline

Zimnik NC, Treadway T, Smith RS, Araneda RC (2013) alpha(1A)-Adrenergic regulation of inhibition in the olfactory bulb. J Physiol 591: 1631–1643. CrossRef Medline